

NATIONAL TRANSPORTATION SAFETY BOARD

Office of Research and Engineering
Materials Laboratory Division
Washington, D.C. 20594



December 23, 2020

MATERIALS LABORATORY FACTUAL REPORT

Report No. 20-049

A. ACCIDENT INFORMATION

Place : Anchorage, Alaska
Date : June 8, 2020
Vehicle : Piper PA-12
NTSB No. : ANC20LA059
Investigator : Brice Banning, AS-ANC

B. COMPONENTS EXAMINED

Fractured rudder from the accident airplane and two fractured rudders from other Piper PA-12 airplanes.

C. DETAILS OF THE EXAMINATION

Rudders from three Piper PA-12 airplanes, including the one from the accident airplane, were submitted for examination as shown in figures 1 through 3. For reference, the rudder from the accident airplane was labeled rudder "A", and the other two rudders were arbitrarily labeled "B" and "C", respectively. The rudder post was fractured at the upper end of the upper hinge barrel attach point on rudder A and approximately ½ inch and 1 inch above the upper hinge barrel on rudders B and C, respectively. The upper portion of the rudder was bent to the left in rudders A and C and to the right in rudder B.

Closer views of the fractures on each of the rudders are shown in figures 1 through 3. The fractures were primarily oriented in a transverse plane, and the cross-section of the tube remained mostly round, consistent with a progressive fracture mechanism such as fatigue under bending loads.¹ Overall, the fracture surfaces were substantially damaged with post-fracture contact damage and rubbing.

Each of the rudder posts was sectioned using a hand-held bandsaw within approximately 3 inches of the fracture surface on each side of the fracture to facilitate closer examinations of the fractures using an optical stereomicroscope. Both sides of the fracture on rudders A and B were smeared, and no evidence of original fracture features were observed. Much of the fracture surface for the rudder C fracture was also damaged, but some areas with relatively undamaged fracture features were identified for closer examination using a scanning electron microscope (SEM).

¹ Given the ratio of wall thickness to tube diameter, an overstress fracture under bending loads would be expected to cause the compression side to buckle, producing a D-shaped cross-section at the fracture location.

The six sectioned rudder post pieces were submerged in a beaker of acetone and cleaned using an ultrasonic cleaner. Both sides of the cleaned fracture from rudder A were examined using an SEM. The fracture surfaces were completely rubbed, and no original fracture features were identified. The upper side of the cleaned fracture from rudder B was also examined using an SEM. The rudder B fracture surface was completely rubbed, and like the fracture surfaces from rudder A, no original fracture features were identified.

The upper fracture surface from rudder C was also substantially damaged, but the SEM revealed areas of original fracture features in the forward right quadrant of the fracture as shown in figure 4. The fracture features near the outer diameter were obliterated by rubbing, but the middle and inner portions of the fracture had arrays of parallel ridges and microcracks consistent with fatigue crack propagation. A closer view of fatigue features is shown in the lower image in figure 4. Unlabeled arrows in figure 4 indicate the direction of fatigue propagation in this area. The orientation and shape of the fatigue features were consistent with fatigue propagation through the thickness from multiple fatigue origins at the outer diameter. On the right side of the rudder post aft of the area shown in figure 4, isolated areas of fatigue features observed between areas of damage were oriented consistent with crack propagation around the circumference away from the origin area at the forward right quadrant. The extent of the fatigue crack propagation and whether additional origin areas may have existed could not be determined due to the extent of fracture surface damage.

The exterior surface of the rudder C rudder post had curving scratches in the painted surface, and the underlying metal was corroded along the lengths of the scratches. The fatigue origin area corresponded to the location of one of the corroded scratches (see figure 3).

Additional transverse cuts were made through the rudder post pieces with the upper sides of the fractures using a water-cooled abrasive saw to produce samples for dimensional measurements and compositional analysis. After the cuts were made, surface coatings on the sectioned pieces were then scraped away using a scalpel to expose the underlying metal. The rudder post from rudder A was painted white, and after starting to remove the paint with a scalpel, large pieces of paint peeled from the surface by hand. The rudder post from rudder B was painted gray with a green primer coating, and the rudder post from rudder C was painted green with a yellow primer coating. The interior surfaces of the rudder posts from rudders A and C were not coated, and loose oxides were removed by briefly sanding with 600-grit sandpaper. The interior surface of the rudder B rudder post was painted gray, and the coating was scraped from the interior using a scalpel.

A sample of the rudder A coating was analyzed using EDS. Spectra were obtained on both the exterior surface and the surface that had mated to the metal substrate. The EDS spectra on both sides had similar peaks with high peaks of titanium, oxygen, and carbon with smaller peaks of iron, nickel, silicon, aluminum, and magnesium. No visual or compositional evidence of a primer was noted in the coating sample from rudder A.

The exterior surface of the rudder A rudder post piece is shown in figure 5 after the paint was removed. The surface had a uniform gray appearance that sparkled when viewed under bright lights. Portions of the surface had a cratered appearance including the area shown in figure 5. The piece shown in figure 5 was further examined using an SEM, and typical surface features are shown in figure 6. The surface had sliding contact features with smooth faces and angular edges consistent with an abrasive-blast treatment. Particles with sharp edges were observed embedded in many of the angular sliding contact areas such as the particle shown in figure 7. The particles were analyzed using energy-dispersive x-ray spectroscopy (EDS), and a typical spectrum is shown in figure 8. The EDS spectra of the embedded angular particles included peaks of iron, silicon, aluminum, magnesium, and oxygen, consistent with the chemical composition of garnet.

Rudder post pieces from rudders B and C were soaked in Cee-Bee paint remover to remove the coatings. A brush and wood scraper were also used to help with the coating removal process. The surfaces with the paint removed had a rough appearance with isolated remnants of primer remaining attached in the surface features. SEM images of the surfaces are shown in figures 9 and 10 showing faceted features consistent with abrasive impacts. Faceted deposits with smooth faces were observed on the surfaces, and EDS analysis of the faceted deposits showed spectra with high peaks of silicon and oxygen consistent with the composition of silica.

The outer diameter of each rudder post was measured using a micrometer across the forward to aft direction and the transverse direction. Additionally, the wall thickness was measured on the forward side of each post using a ball-flat micrometer. Results of the measurements are listed in table 1 and had values consistent with nominal tube dimensions specified in the engineering drawings for the rudder post used on the Piper PA-12 and Piper PA-18 airplanes. According to those engineering drawings, the tube for the rudder post was specified as a 7/8-inch tube with a tube wall thickness of 0.035 inch.

Table 1. Selected Rudder Post Dimensions

Rudder	Outer Diameter Forward – Aft (inch)	Outer Diameter Side – Side (inch)	Tube Wall Thickness (inch)
A	0.877	0.879	0.0379
B	0.879	0.876	0.0369
C	0.880	0.879	0.0355

The engineering drawing for the PA-12 rudder shows two cylinders welded to the forward side of the rudder post for the rudder hinges. The inside diameters of the hinge cylinders are between 0.249 inch and 0.251 inch as listed in the engineering drawing. A micrometer was used to measure the inside diameters of the upper and lower rudder hinge cylinders on each of the submitted rudders. The diameter was measured in the transverse plane at the upper and lower sides of each hinge cylinder, and results are listed in table 2. The inside diameters measured on the lower hinge cylinders were mostly

within the diameter range specified in the engineering drawing, and the inside diameters for the upper hinge cylinders all measured 0.002 inch to 0.008 inch larger than the corresponding measurement on the lower hinge.

Table 2. Rudder Hinge Inside Diameter Measurements

Rudder	Upper Hinge, Upper End (inch)	Upper Hinge, Lower End (inch)	Lower Hinge, Upper End (inch)	Lower Hinge, Lower End (inch)
A	0.253	0.256	0.251	0.252
B	0.257	0.253	0.249	0.251
C	0.256	0.256	0.251	0.251

According to engineering drawings, the rudder post for the Piper PA-12 airplane was originally manufactured from AISI 1025 carbon steel. In a Piper engineering change order (ECO) dated June 3, 1974, the specified material for the rudder post was changed to normalized AISI 4130 low-alloy steel. The ECO allowed for existing in-process and completed parts to be used to depletion. In order to determine the compositions of the rudder posts from the submitted rudders, sides of the sectioned pieces from rudders B and C were ground using 240-grit abrasive paper to expose an area for testing (the surface of the rudder A piece was tested as found after peeling the paint away). The compositions of the rudder posts were then analyzed using an Olympus Vanta C-Series alloy analyzer. The material associated with all three rudder posts was identified as carbon steel, and detected levels of chromium and molybdenum were less than 1/10 of the composition ranges associated with AISI 4130 low-alloy steel.

Hardness was measured on the each of the rudder post pieces. The surface of the tube was ground with silicon-carbide abrasive paper up to a grit size of 600 grit to smooth the surface for superficial hardness testing with a Rockwell indenter. Measured hardness values were adjusted for curvature in accordance with standard ASTM E18.² A table in standard ASTM A370 was used to convert the tested hardness values to the Rockwell B scale and to estimate the approximate ultimate tensile strength of the rudder post material.³ Results of the hardness tests and converted values are listed in table 3. All hardness values were less than the expected minimum hardness for normalized AISI 4130 steel. The Air Force – Navy – Commerce Bulletin ANC-5 lists properties for alloy 1025 steel tube, and the ultimate tensile strength for general design purposes is listed as 55 ksi.⁴

² ASTM Standard E18, *Standard Test Methods for Rockwell Hardness of Metallic Materials*, ASTM International, West Conshohocken, PA, 2020, www.astm.org

³ ASTM Standard A370, *Standard Test Methods and Definitions for Mechanical Testing of Steel Products*, ASTM International, West Conshohocken, PA, 2020, www.astm.org

⁴ Air Force – Navy – Commerce Bulletin ANC-5, *Strength of Metal Aircraft Elements*, US Department of Defense (1951).

Table 3. Rudder Post Hardness and Approximate Tensile Strength

Rudder	Measured Hardness* (HR30-TW)	Converted Hardness (HRB)	Approximate Tensile Strength (ksi)
A	65.6	74	65
B	63.6	71	62
C	49.7	50	**

*Including adjustment for specimen curvature.

**An approximate tensile strength is not associated with this hardness value in ASTM Standard A370.

In a Piper engineering order (EO) dated June 15, 1988, an aluminum alloy shim was added to the interior of the rudder post at the lower end where it is attached to the rudder arm.⁵ On October 4, 1988, the shim material was changed from the aluminum alloy to a stainless steel alloy. A shim was observed at the lower end of the rudder post in rudder A (see figure 11). A scalpel was used to shave a sample of the shim onto a carbon-coated stub for EDS analysis. Results showed a spectrum with a high peak of aluminum and small peaks of copper and magnesium, consistent with the aluminum alloy shim material specified in the June 1988 EO. No shims were observed in the rudder posts for rudders B and C.

Matthew R. Fox, Ph.D.
Senior Materials Engineer

⁵ The rudder arm is attached to the lower end of the rudder post. The outer ends of the rudder arm are connected to the tail wheel by a spring linkage.

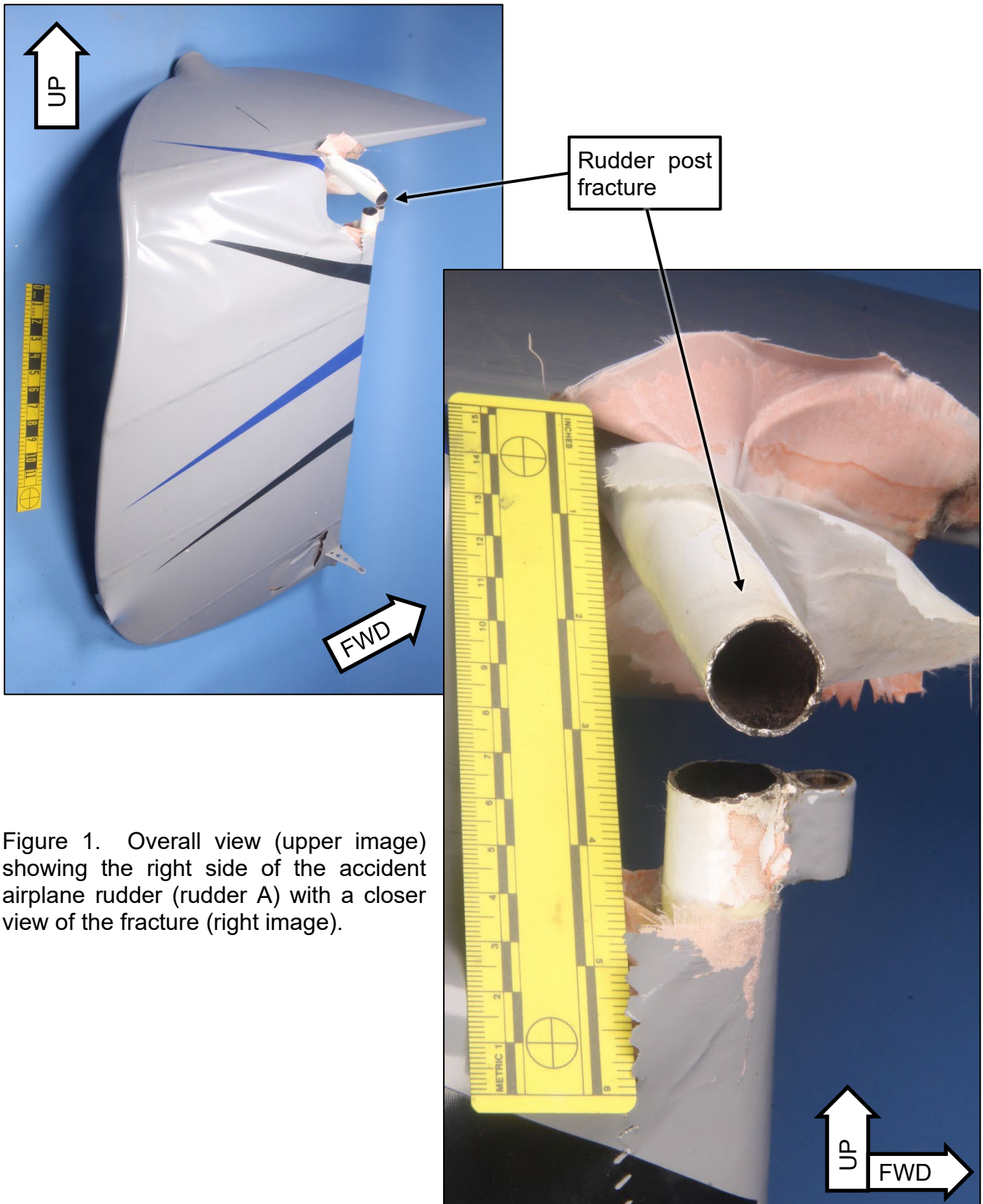
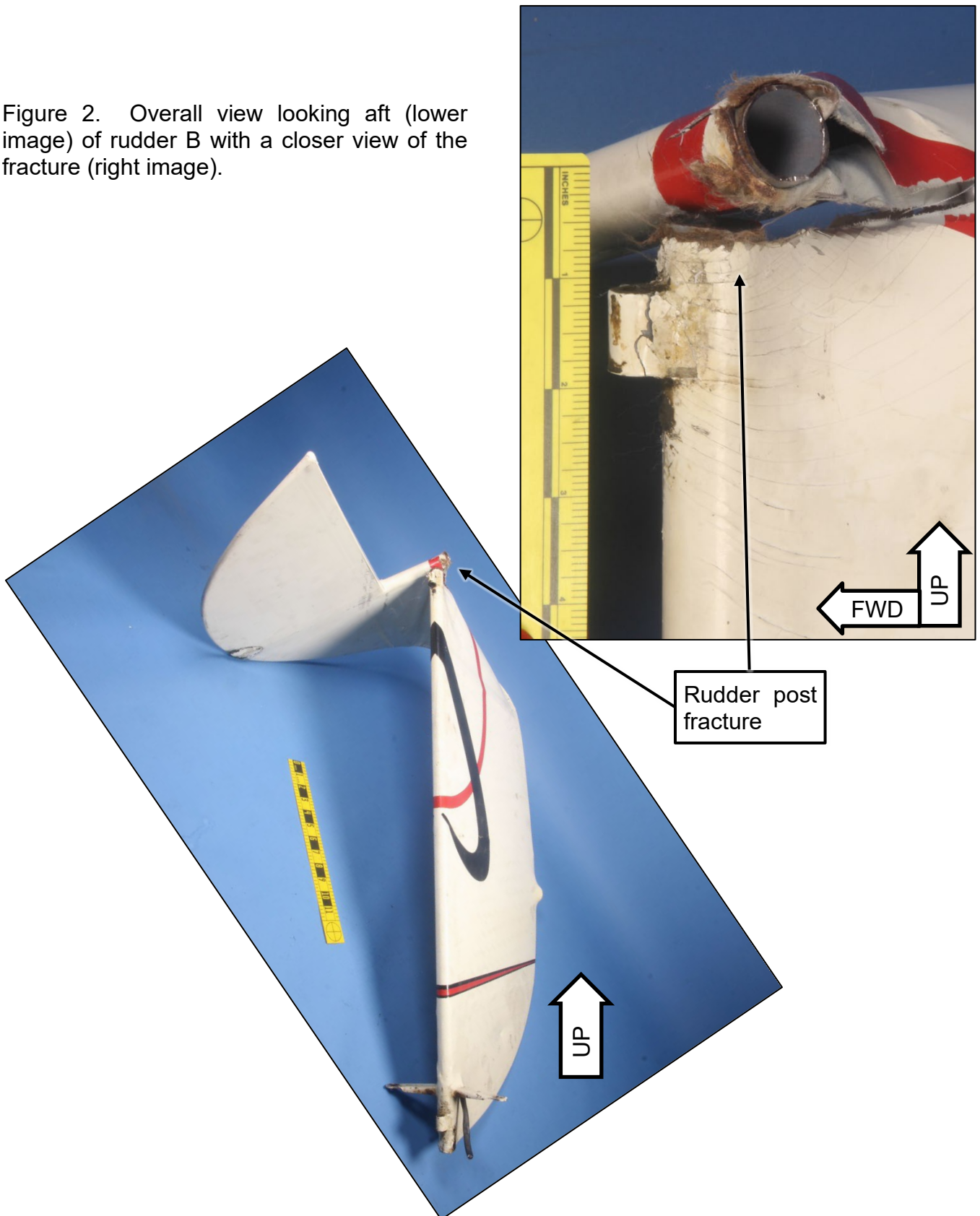


Figure 1. Overall view (upper image) showing the right side of the accident airplane rudder (rudder A) with a closer view of the fracture (right image).

Figure 2. Overall view looking aft (lower image) of rudder B with a closer view of the fracture (right image).



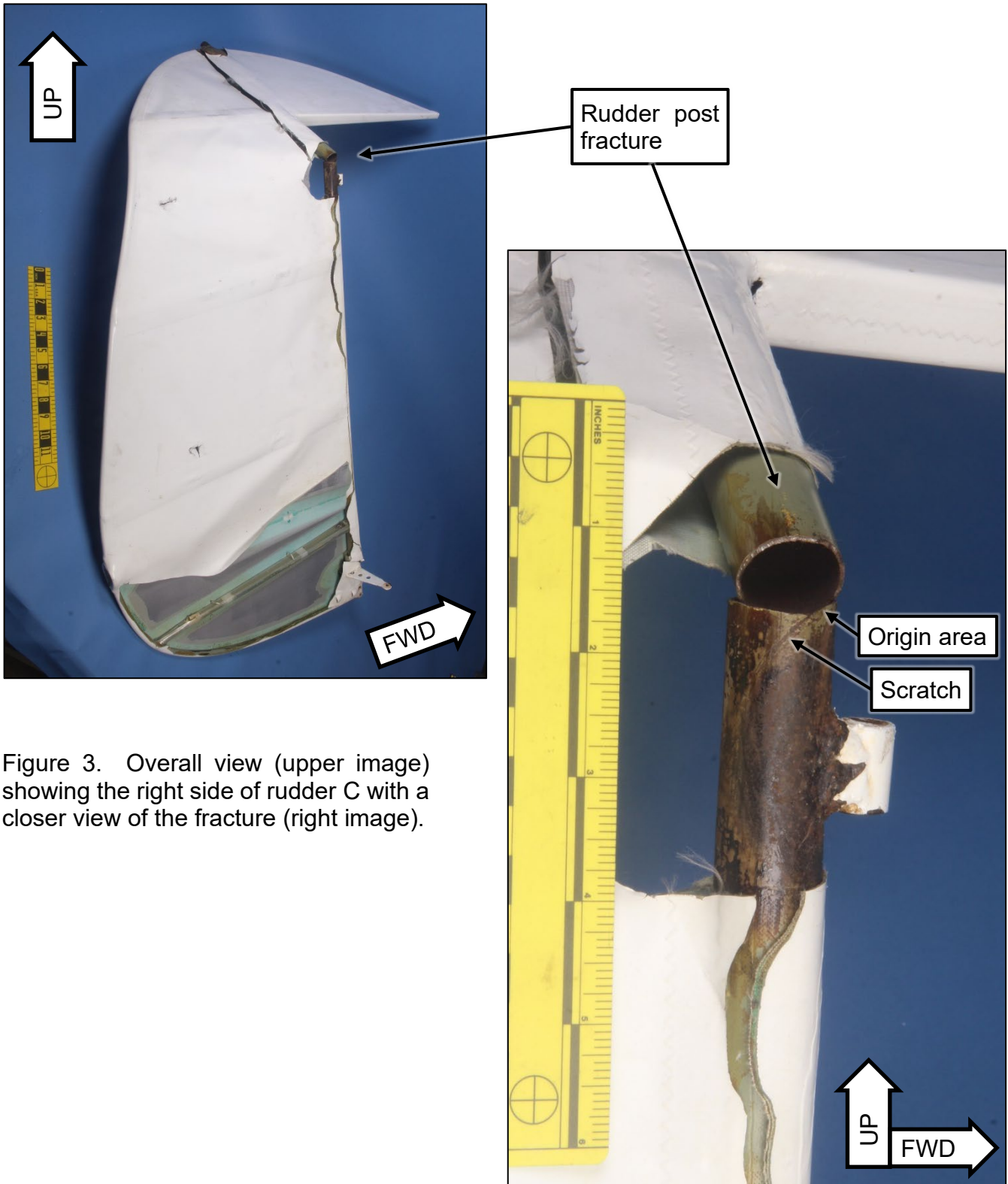


Figure 3. Overall view (upper image) showing the right side of rudder C with a closer view of the fracture (right image).

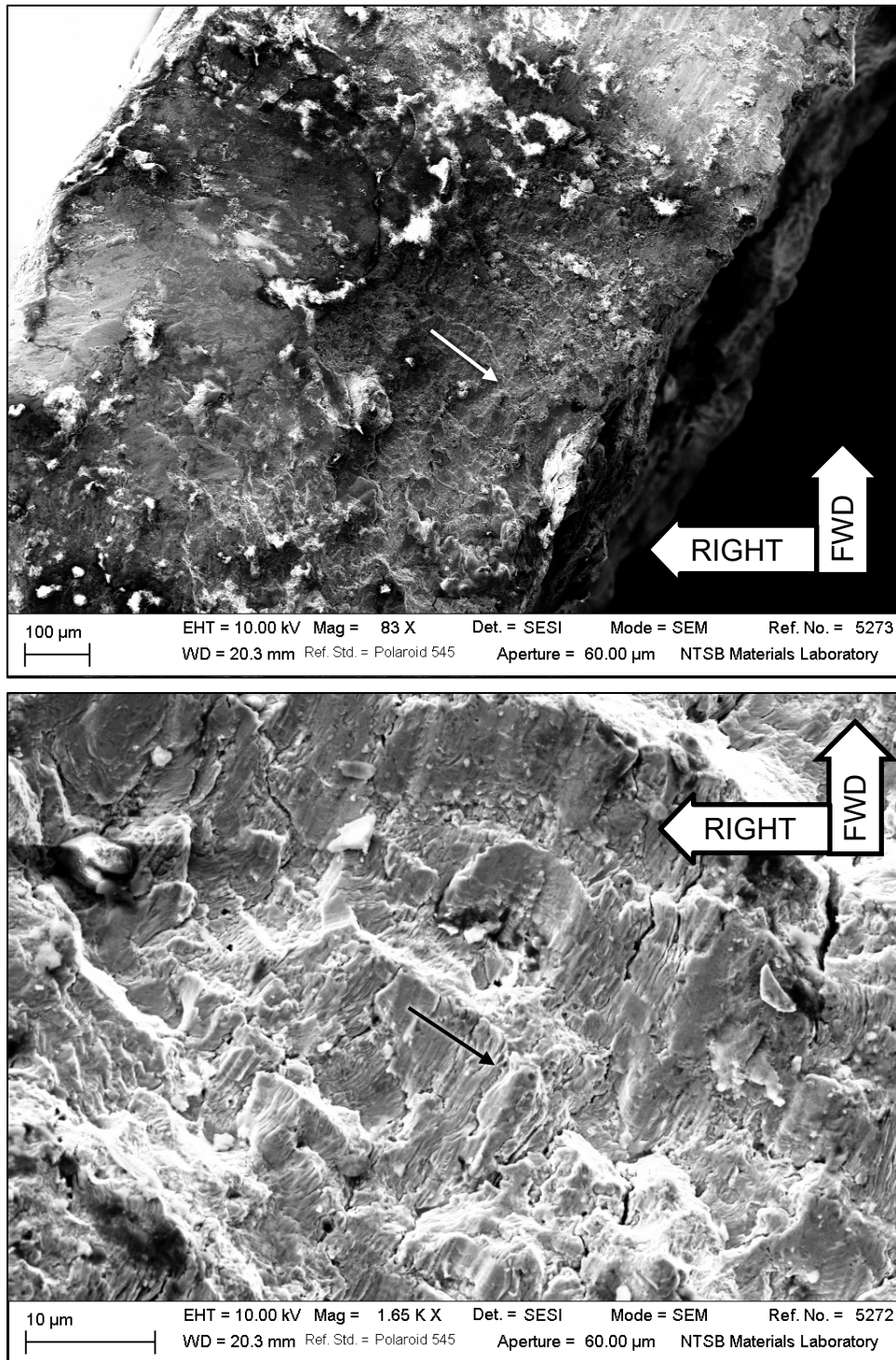


Figure 4. SEM images of the upper side of the rudder post fracture in rudder C after ultrasonic cleaning with acetone. The upper image shows an area of the forward right quadrant, and the lower image shows a closer view of fatigue fracture features. Unlabeled arrows indicate the general fatigue crack propagation direction.



Figure 5. Section of rudder post from rudder A approximately 1 inch above the fracture after paint was removed showing pitting on the right side of the post.

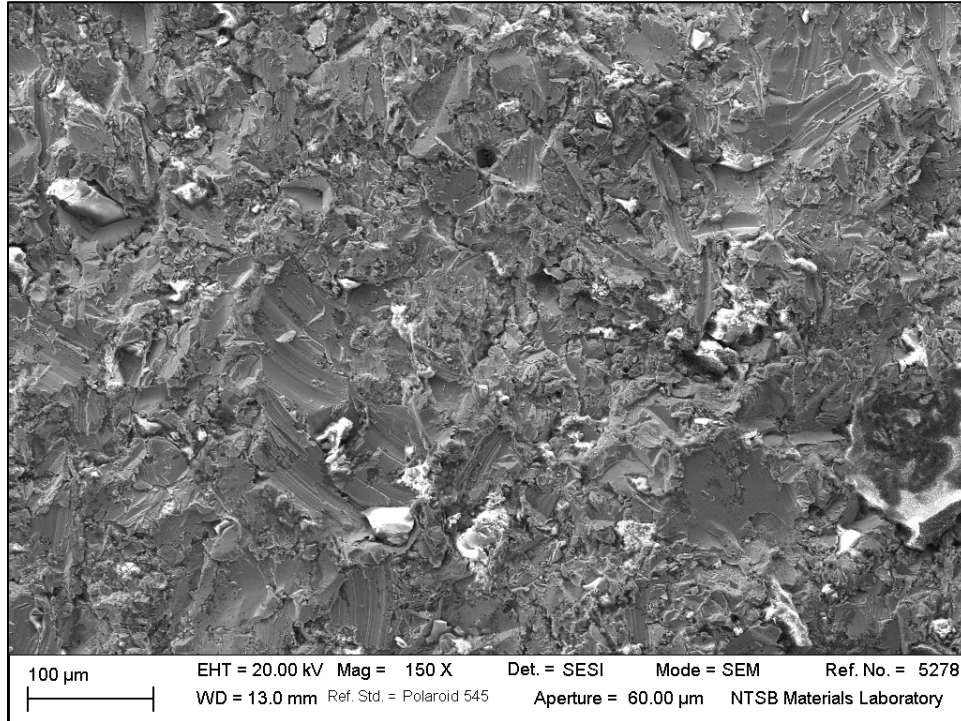


Figure 6. SEM image of the rudder post exterior surface on the rudder A piece shown in figure 5.

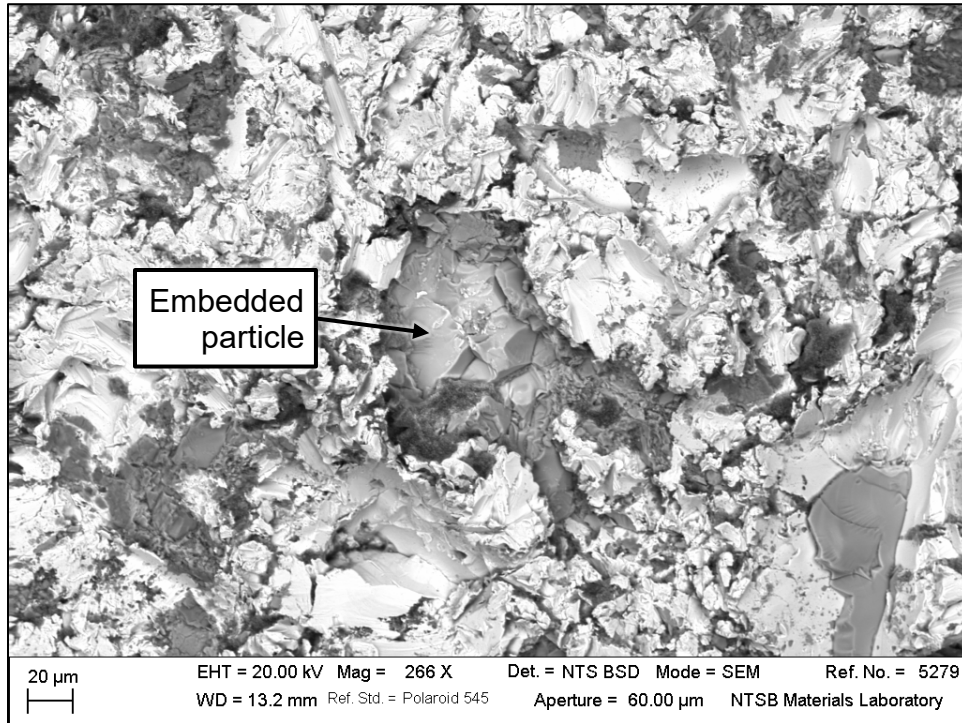


Figure 7. SEM image of a particle embedded in the surface of the rudder A rudder post.

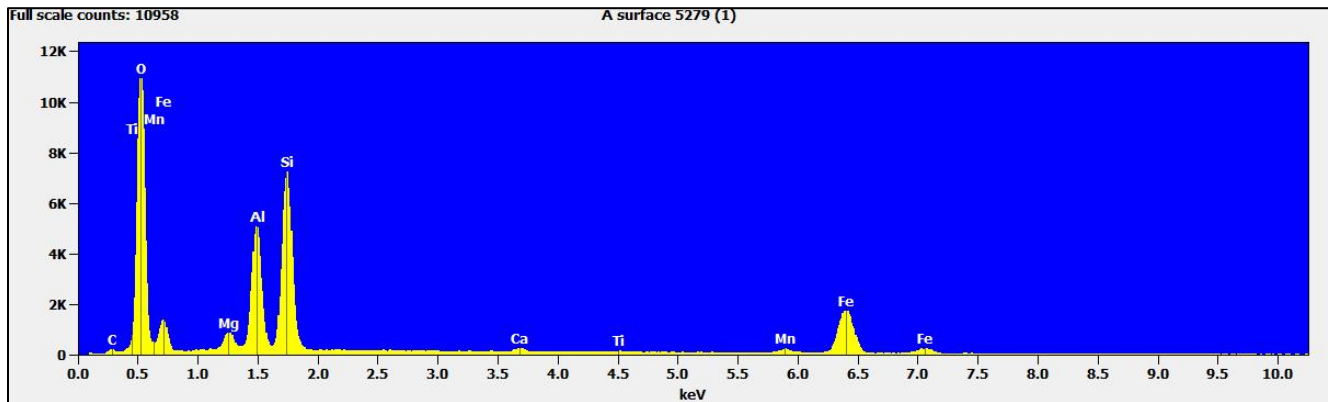


Figure 8. EDS spectrum for the particle shown in figure 7.

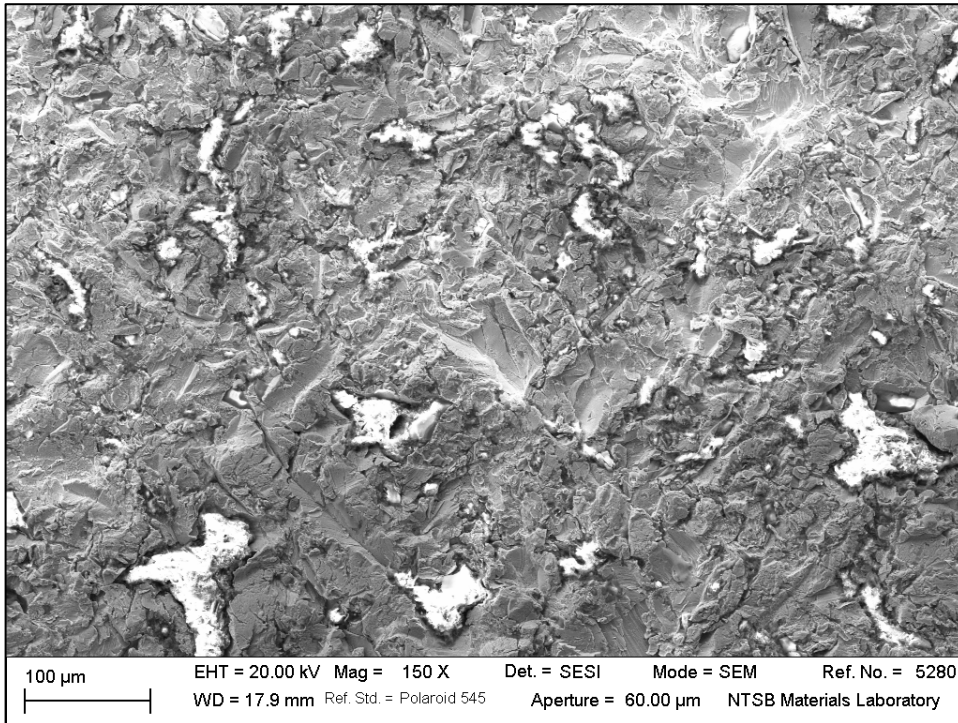


Figure 9. SEM image of the rudder post exterior surface on the rudder B piece.

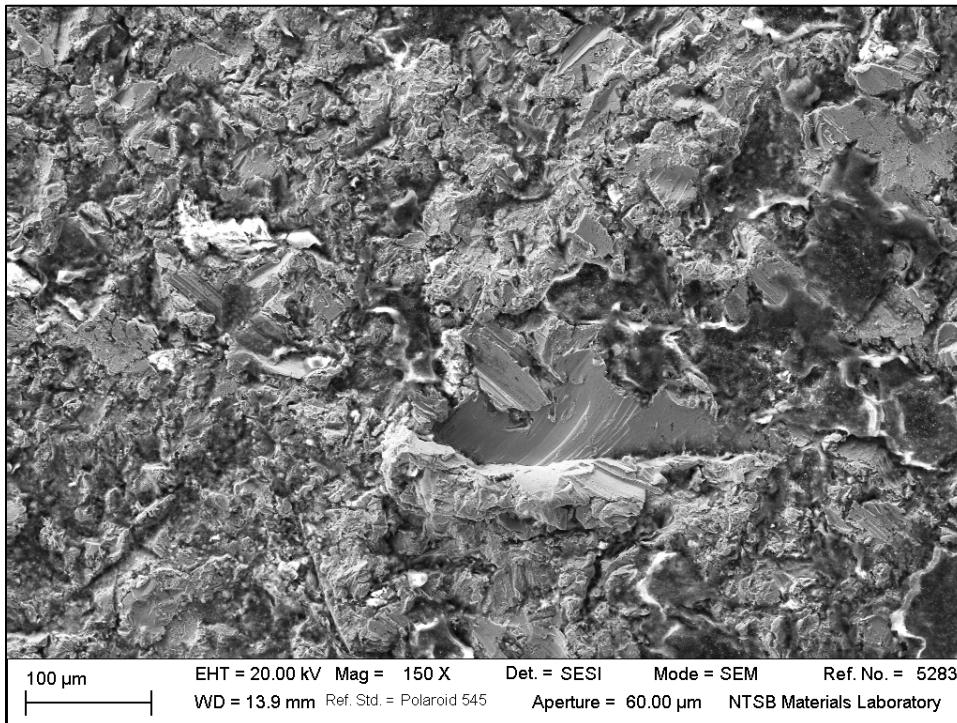


Figure 10. SEM image of the rudder post exterior surface on the rudder C piece.

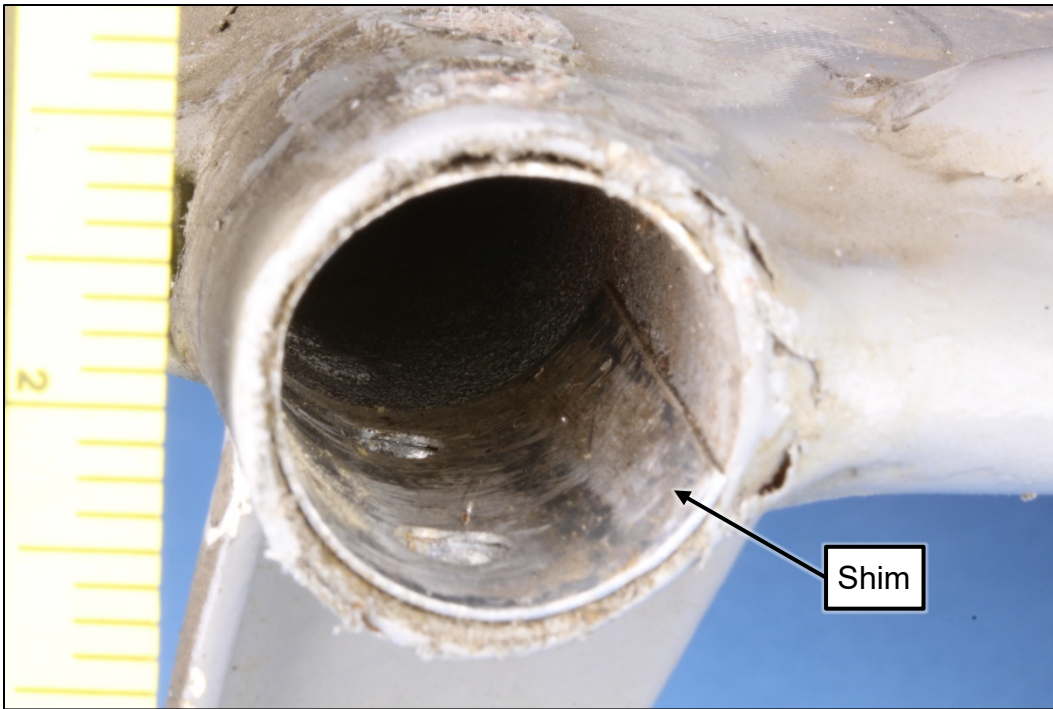


Figure 11. Lower end of rudder A showing the shim installed inside the rudder post.